Electron avalanches and diffused γ-mode in radio-frequency capacitively coupled atmospheric-pressure microplasmas

D. W. Liu, F. Iza,[a] and M. G. Kong
Department of Electronic and Electrical Engineering, Loughborough University, Leicestershire LE11 3TU, United Kingdom

(Received 1 June 2009; accepted 6 July 2009; published online 20 July 2009)

Space-, time- and wavelength-resolved optical emission profiles suggest that the helium emission at 706 nm can be used to indicate the presence of high energy electrons and estimate the sheath in helium rf discharges containing small concentration of air impurities. Furthermore, the experimental data supports the theoretical predictions of energetic electron avalanches transiting across the discharge gap in rf microdischarges and the absence of an α-mode. Nonetheless, microdischarges sustained between bare metal electrodes and operating in the γ-mode can produce diffuse glowlike discharges rather than the typical radially constricted plasmas observed in millimeter-size rf atmospheric-pressure γ discharges. © *2009 American Institute of Physics*.
[DOI: 10.1063/1.3186073]

Microplasmas represent a new realm in plasma physics that is attracting growing attention for their potential economic and technological impact.[1–4] In particular, microplasmas operating at atmospheric pressure are of special interest as they enable chamberless operation and do not require costly vacuum systems.

In this letter, we present experimental data aimed at revealing underlying principles governing atmospheric-pressure rf microplasmas and at validating existing theoretical predictions. In particular, it has been suggested that as the gap size decreases, the size of the quasineutral bulk plasma reduces and the plasma becomes dominated by sheaths.[5–7] Furthermore, simulations of atmospheric pressure rf microdischarges suggest that these plasmas can only be sustained in the so-called γ-mode and that energetic beams of electrons transit the discharge gap reaching the electrodes with sufficient energy as to influence the surface chemistry.[2,7] In this letter, we present experimental evidence that support these theoretical predictions.

The experimental setup used in this work consists of two water-cooled parallel stainless steel electrodes, each being 2 cm in diameter. The discharge gap is varied between 300 μm and 2 mm and the system is housed in a Perspex box. Helium (99.95% purity) flows into the box at 5 slm, and nitrogen and oxygen are present as impurity traces ($<$500 ppm). A function generator (Tektronix AFG 3102), a rf power amplifier (Amplifier Research 500A100A), and a house-built matching network are used to deliver 6.78 MHz power to the discharge. Similar results have been obtained for 13.56 and 27 MHz discharges (data not shown). The current and voltage across the discharge are measured with a wideband current probe (Pearson Current Monitor 2877), a wideband voltage probe (Tektronix P5100), and a digital oscilloscope (Tektronix TDS 5054B). Finally, an intensified charge-coupled device camera (Andor i-Star DH720) and optical filters (Thorlabs FWHM 10 nm) are used to take discharge images.

Interpretation of the experimental data is aided by simulation results. The simulation model used is an extension of the one described in Ref. 8, and incorporates helium-nitrogen chemistry and emission from the $N_2^+(B^2\Sigma_g^+)$ and $He(^3S_1)$ excited states. These correspond to the emissions at 391 and 706 nm, respectively. The model solves the electron energy equation and reaction rates as a function of the electron mean energy are obtained using the Boltzmann solver Bolsig + (Ref. 9) and cross section data from Refs. 9–12. Despite the limitations of fluid models,[13] this simulation approach has been used in other studies of atmospheric-pressure discharges reaching good agreement with selected experimental data.[8,13–15]

Figure 1 shows the current-voltage (I-V) curve of atmospheric-pressure He rf discharges in different gaps. As the discharge gap decreases, the voltage required to ignite and sustain the discharge also decreases. The reduction, however, is not proportional to the reduction in gap size and higher electric fields are required to ignite smaller gaps.[16] This tendency is attributed to the increasing surface to volume ratio and thereby electron loss to the electrodes as the gap is reduced. One can also note that the dynamic plasma impedance (slope of the I-V curve) decreases as well. The last point of each curve, i.e., the point of maximum current, corresponds to the discharge condition right before the transition to the constricted γ-mode.[8,17,18]

Figure 2 shows the spatio-temporal evolution of the plasma optical emission as a function of the gap size. The

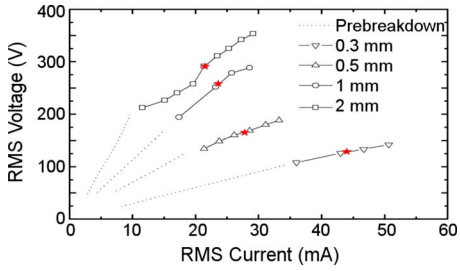

FIG. 1. (Color online) Current-voltage curves of diffused glowlike rf helium discharges in various gaps. Stars indicate conditions for Fig. 2.

[a]Author to whom correspondence should be addressed. Electronic mail: f.iza@lboro.ac.uk.

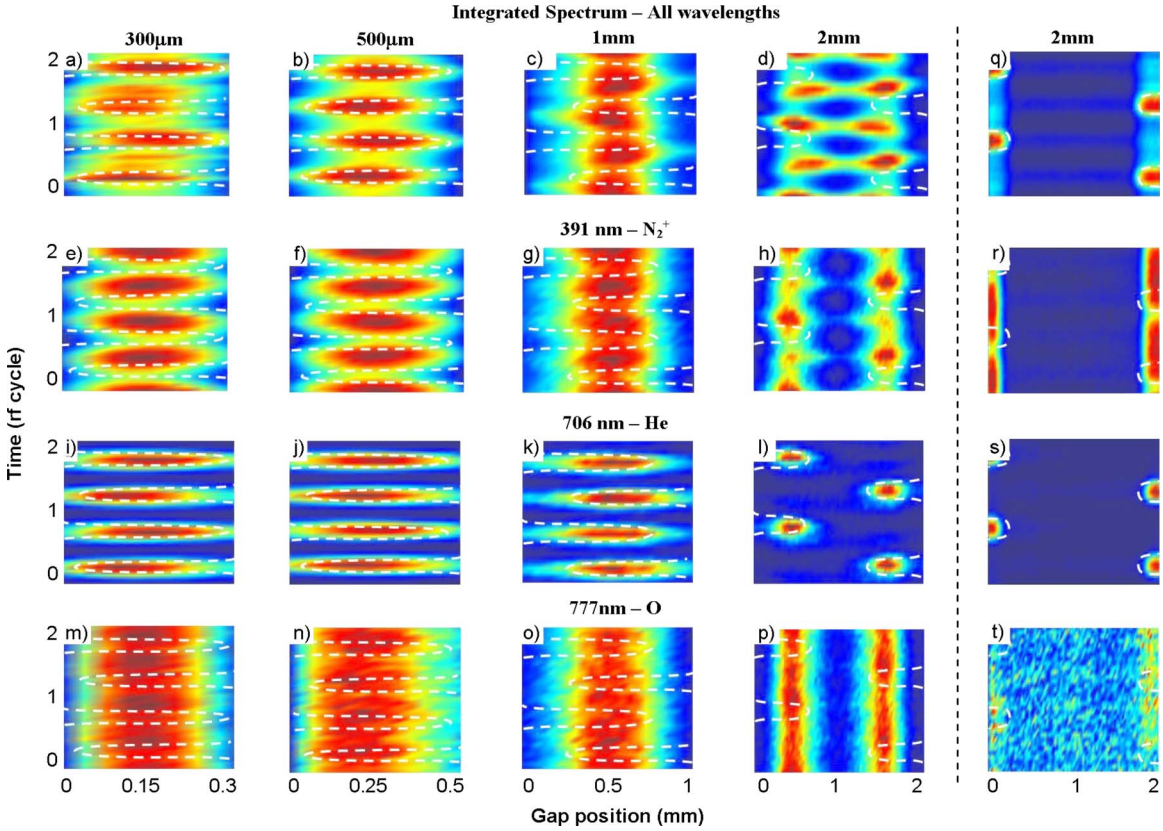

FIG. 2. (Color online) Spatiotemporal evolution of the optical emission of [(a), (e), (i), and (m)] 300 μm, [(b), (f), (j), and (n)] 500 μm, [(c), (g), (k), and (o)] 1mm, and [(d), (h), (l), and (p)] 2 mm rf-diffused glowlike discharges: [(a)–(d)] wavelength-integrated, [(e)–(h)] N_2^+ 391 nm, [(i)–(l)] He 706 nm, and [(m)–(p)] O 777 nm. [(q)–(t)] Emission pattern in the constricted γ-mode. White lines indicate the estimated sheath region based on the emission pattern of 706 nm and are shown to guide the eye. Images are not normalized to highlight their pattern rather than their relative intensity. Strong emission regions are shown in red whereas regions of no emission are shown in dark blue.

discharge conditions are marked with red stars in Fig. 1 and the patterns shown are characteristic for each gap size, i.e., no qualitative changes are observed if the current is changed within the range shown in Fig. 1. The emission pattern in a constricted γ-mode is also shown in Fig. 2 for completeness. The all-wavelength (spectrum-integrated) optical emission as well as the emission at 391 (N_2^+), 706 (He), and 777 nm (O) are shown. The radiative decay lifetimes of the upper states for these three transitions are 60, 64, and 27 ns, respectively,[19] and the actual lifetime is even shorter due to collisional quenching. Since the lifetimes are shorter than the rf period (148 ns), the spatio-temporal evolution of the emission can be used to infer when and where $N_2^+(B^2\Sigma_g^+)$, $He(^3S_1)$, and $O(^5P_1)$ are populated.

For large gaps (1–2 mm), the all-wavelength emission pattern [Figs. 2(c) and 2(d)] is similar to that of N_2^+ [Figs. 2(e)–2(h)] despite the low nitrogen concentration in the neutral gas (<0.05%). This is not surprising as small concentrations of impurities in a helium discharge can significantly affect the plasma.[20] Indeed the emission spectrum (not shown) is dominated by nitrogen molecular and ionic bands. It is interesting to note, however, that not only the emission of helium at 706 nm is less intense than the nitrogen emission, but it also has a different pattern [compare Figs. 2(g) and 2(h) with Figs. 2(k) and 2(l)]. The emission patterns indicate that nitrogen ion excitation takes place outside the sheaths whereas helium excitation occurs predominantly inside the sheaths. Simulation results also capture this behavior and provide insights onto the different excitation mechanisms of $N_2^+(B^2\Sigma_g^+)$ and $He(^3S_1)$. Whereas $N_2^+(B^2\Sigma_g^+)$ is excited by the combined action of He metastables (Penning ionization of N_2) and low energy electrons (excitation of N_2^+ $(X^2\Sigma_g^+)$ by electrons with $\varepsilon > 3$ eV), helium excitation requires high energy electrons ($\varepsilon > 22$ eV) because the main excitation mechanism is ground state electron impact excitation. As a result, 391 nm emission peaks outside the sheath where a relatively large number of electrons can reach 3 eV whereas 706 nm peaks inside the sheath where a significant number of electrons can reach >22 eV. Finally it can also be observed that the spatio-temporal emission profile of the atomic oxygen at 777 nm [Figs. 2(o) and 2(p)] is yet different to that of nitrogen and helium. The weak temporal dependence of the 777 nm emission pattern suggests that $O(^5P_1)$ is mainly populated by collisions involving long-lived metastable states. Underpinning the mechanisms leading to these different emission patterns are beyond the scope of this letter and will be addressed in a separate manuscript. Here it is only noted that experimental and computational data suggest that helium emission at 706 nm in He discharges with a small concentration of impurities can be used to indicate the presence of energetic electrons ($\varepsilon > 22$ eV), and thereby the 706 nm emission pattern is closely related to that of the sheaths.

As the gap size is reduced, the bulk plasma shrinks and the sheaths extend across a larger portion of the gap [Figs. 2(i)–2(l)]. This supports earlier computer simulation results.[5–7] As a result, the bright emitting regions above the

electrodes get closer together and eventually overlap in the center of the discharge [compare Figs. 2(d) and 2(a)–2(c)]. It is interesting to note, however, that as the gap decreases not only the emission patterns associated with each sheath approach each other, but a shift in dominant species also takes place. Whereas in the 1–2 mm gap discharges, the overall emission is dominated by nitrogen (see the pattern similarity between Figs. 2(c) and 2(d) and Figs. 2(g) and 2(h)], in the 300–500 μm discharges the pattern of the overall emission agrees with that of helium [see Figs. 2(a) and 2(b) and Figs. 2(e) and 2(f)]. This is also supported by the emission spectrum (not shown) that shows a decrease in nitrogen emission and an increase in helium lines.

Figure 2 also supports the theoretical prediction regarding the presence of electron avalanches crossing the discharge gap and reaching the opposite electrode[7] [compare Figs. 2(i) and 2(l) and note how 706 nm emission extends across the discharge gap as the gap size is reduced). These avalanches are initiated by secondary electrons as well as penning ionization inside the sheaths.[8]

Another theoretical prediction made in Refs. 2 and 7 was that rf microdischarges can only operate in the γ-mode, i.e., the discharge is sustained mainly by ionization avalanches in the sheaths. This prediction was based on one-dimensional analyses and therefore did not address the possible radial constriction of the discharge. It is normally believed that operation in the γ-mode at atmospheric pressure leads to a constriction of the discharge.[17,18] The discharges described in this letter, however, are diffuse unless otherwise noted. Therefore, the question of whether microdischarges operate in the α-mode against theoretical predictions in 2 and 7 or in a diffuse (rather than the typical constricted) γ-mode arises.

The emission pattern at 706 nm [Figs. 2(i)–2(l)] indicates that electron avalanches as those needed to sustain the discharge in the γ-mode actually exist in microdischarges but does not prove that the avalanches are the main ionization mechanism of the discharge. In fact emission at 706 nm is also recorded in the sheaths of millimeter-gap discharges yet they operate in the α-mode. It is noted, however, that in large ($\sim$2 mm) constricted γ discharges, the emission pattern also agrees with that at 706 nm [Figs. 2(q)–2(t)], suggesting that microdischarges operate in a diffuse γ-mode because their emission is also dominated by He [compare Figs. 2(a) and 2(b) and Figs. 2(i) and 2(j)]. Since electron generation cannot be measured directly, computer simulations are used to probe this further.

Figures 3(a)–3(c) show the 706 nm emission pattern in small (500 μm) and large (2 mm) gaps predicted by computer simulations. These agree well with the experimental data shown in Figs. 2(j), 2(l), and 2(s). Furthermore, Figs. 3(d)–3(f) show the electron generation rate in the two gaps. In the 2 mm gap, the emission at 706 nm and the electron generation rate are different in the α-mode [Figs. 3(a) and 3(d)], i.e., avalanches in the sheaths are responsible for the excitation of helium atoms but ionization (mostly nitrogen) is governed by bulk electrons interacting with the oscillating sheaths.[8] In the γ-modes and in small gaps, however, the emission at 706 nm and the electron generation rate have a very similar pattern indicating that avalanches in the sheaths are responsible for the ionization of the gas [Figs. 3(b) and 3(c) and Figs. 3(e) and 3(f)]. Therefore, we conclude that rf

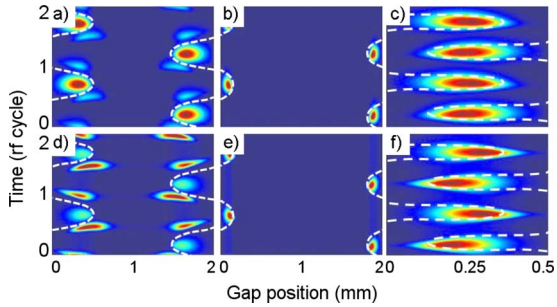

FIG. 3. (Color online) Simulated spatio-temporal evolution of the [(a)–(c)] 706 nm He optical emission and [(d)–(f)] electron generation rate in [(a) and (d)] 2 mm α-mode, [(b) and (e)] 2 mm γ-mode, and [(c) and (f)] 500 μm rf He+0.04% N_2 discharges.

microdischarges operate in a diffused γ-mode and that only at high power the microdischarge constricts radially as it is typically observed in millimeter-size atmospheric-pressure γ discharges.[17,18] The reasons for the constriction are subject of future investigations.

In conclusion, experimental results suggest that emission at 706 nm in helium rf discharges with admixtures of air indicate the presence of high energy electrons and can be used to estimate the sheath width. Furthermore, experimental data support the theoretical predictions of energetic electron avalanches transiting across microdischarges and the absence of an α-mode. Instead of an α-mode, experimental and simulation data suggest microplasmas operate in a diffuse glow-like γ-mode.

The authors acknowledge the support received from the Engineering and Physical Sciences Research Council, U.K.

[1]"Plasma Science: Advancing Knowledge in the National Interest," National Academies Report, Washington, D.C., National Academies Press, 2007.
[2]F. Iza, G. J. Kim, S. M. Lee, J. K. Lee, J. L. Walsh, Y. T. Zhang, and M. G. Kong, Plasma Processes Polym. **5**, 322 (2008).
[3]K. Tachibana, Trans Electr. Electron. Eng. **1**, 145 (2006).
[4]K. H. Becker, K. H. Schoenbach, and J. G. Eden, J. Phys. D **39**, R55 (2006).
[5]M. J. Kushner, J. Phys. D **38**, 1633 (2005).
[6]J. J. Shi and M. G. Kong, Phys. Rev. Lett. **96**, 105009 (2006).
[7]F. Iza, J. K. Lee, and M. G. Kong, Phys. Rev. Lett. **99**, 075004 (2007).
[8]D. W. Liu, F. Iza, and M. G. Kong, Appl. Phys. Lett. **93**, 261503 (2008).
[9]G. J. M. Hagelaar and L. C. Pitchford, Plasma Sources Sci. Technol. **14**, 722 (2005).
[10]Y. Ralchenko, R. K. Janev, T. Kato, D. V. Fursa, I. Bray, and F. J. de Heer, At. Data Nucl. Data Tables **94**, 603 (2008).
[11]Z. Lianzhu, Z. Shuxia, and M. Xiulan, Plasma Sci. Technol. **10**, 455 (2008).
[12]A. V. Kosarim, B. M. Smirnov, M. Capitelli, and R. Celiberto, Chem. Phys. Lett. **414**, 215 (2005).
[13]H. C. Kim, F. Iza, S. S. Yang, M. Radmilovic-Radjenovic, and J. K. Lee, J. Phys. D **38**, R283 (2005).
[14]Q. Wang, D. J. Economou, and V. M. Donnelly, J. Appl. Phys. **100**, 023301 (2006).
[15]P. S. Kothnur and L. L. Raja, J. Appl. Phys. **97**, 043305 (2005).
[16]J. L. Walsh, Y. T. Zhang, F. Iza, and M. G. Kong, Appl. Phys. Lett. **93**, 221505 (2008).
[17]J. J. Shi and M. G. Kong, Appl. Phys. Lett. **90**, 101502 (2007).
[18]S. Y. Moon, J. K. Rhee, D. B. Kim, and W. Choe, Phys. Plasmas **13**, 033502 (2006).
[19]NIST Atomic Spectra Database, http://physics.nist.gov/PhysRefData/ASD/.
[20]T. Martens, A. Bogaerts, W. J. M. Brok, and J. V. Dijk Appl. Phys. Lett. **92**, 041504 (2008).